Received: 8 April 2022 | Revised: 6 October 2022 | Accepted: 6 October 2022

DOI: 10.1111/joa.13782

Journal of Anatomy ANATOMICAL SOCIETY WILEY

ORIGINAL ARTICLE

Proximal ear hole injury heals by limited regeneration during the early postnatal phase in mice

René Fernando Abarca-Buis | Edgar Krötzsch

Laboratory of Connective Tissue, Centro Nacional de Investigación y Atención de Quemados, Instituto Nacional de Rehabilitación "Luís Guillermo Ibarra Ibarra", Ciudad de México, Mexico

Correspondence
René Fernando Abarca-Buis, Laboratory of Connective Tissue, Centro Nacional de Investigación y Atención de Quemados, Instituto Nacional de Rehabilitación "Luís Guillermo Ibarra Ibarra", Av. México-Xochimilco No. 298, Col. Arenal de Guadalupe, Alcaldía Tlalpan, C.P. 14389, Ciudad de México, Mexico.
Email: rabarca@inr.gob.mx

Abstract

Ear pinna is a particular feature of mammals that shows several repair responses depending on age. Two millimeter hole made in the pinna of middle-aged female mice heals due to partial reconstitution of new tissues (limited regeneration), whereas a hole punched in the ear of young mice forms a scar tissue. In these studies, the injury is made in the center of the ear pinna, but little is known about the type of reparative response along the proximodistal polarity of the ear. This study evaluated the effect of pinna polarity, age, and sex in the ear hole-repairing response in Balb/c mice. Proximal injuries were repaired more efficiently by limited regeneration than wounds made in the middle region. Non-injured ear histological analysis revealed a higher presence of muscle, adipose tissue, cartilage, and larger blood vessels in the proximal ear area, which could influence ear hole closure by limited regeneration. To evaluate the healing response during ear growth, we punched a standard hole in the proximal area of the ear on postnatal day 21 and 8-month-old mice (adults). Thirty-five days after the wound, both groups reached the same wound closure, despite the greater proportional size of holes made in the younger mice. Ear growth also improved ear hole closure in male mice. These results suggest that ear growth accelerates hole closure, providing an example of enhanced regenerative abilities in growing structures. Finally, hole closure kinetics in the growing ear indicated an early re-differentiation phase exhibited at 14 days post-wound. In conclusion, ear topography and growth positively influenced the healing response to ear holes, making it a tractable model to study in mammals.

KEYWORDS
ear growth, ear hole injury, elastic cartilage, limited regeneration, mammalian regeneration, RRID:AB_10971844, RRID:AB_1658868, RRID:AB_2336413, RRID:AB_2536522, RRID:AB_262054, RRID:AB_2630356, RRID:AB_778028, RRID:MGI:2160915

1 | INTRODUCTION

Ear pinnae are a mammal-specific trait. Fossil evidence indicates that the functional mammal ear was present around 120 million years ago (Martin et al., 2015), as shown by the exceptionally preserved ear pinna of the primitive eutriconodont *Spinolestes xenarthrosus*. Because Monotremata lack ear pinnae, it is assumed that this structure arose and evolved after the divergence of this group from the rest of mammals, approximately 220 million years ago (Madsen, 2009; Martín-Abad et al., 2016). The functions of pinnae are to identify and localize sound, amplify high frequencies, and filter different sounds selectively (Heffner & Heffner, 2016, 2018). In addition, has been considered that in certain mammals, this structure has evolved to maintain the homeothermy in part, due to its

large and vascularized surface area (Webster, 1966). The basic shape of the external ear resembles a funnel cut in half, with dorso-ventral and proximodistal axes. The proximal region is close to the external auditory canal/acoustic meatus and is generally thicker than the distal portion localized in the pinna tip.

Interestingly, regeneration which is the ability of a fully developed organism to replace lost part (Wolpert et al., 2002) is shown by some mammalian species after a hole is inflicted in the ear pinnae. This observation was reported in 1953 by Markelova when she discovered that holes punched in rabbit ears heal by filling the hole with the previously lost tissues (Goss & Grimes, 1972; Rajnoch et al., 2003). Further, quantitative and qualitative analysis of this model revealed that contraction was not the main process contributing to ear regeneration; rather, cells located in the margin of the hole proliferated to form a structure called blastema, growing centripetally to close the ear wound (Joseph & Dyson, 1966). Additionally, interaction between different types of ear tissues is essential to promote rabbit ear regeneration; this was described in experiments substituting ear skin or deleting the cartilage (Goss & Grimes, 1972). Subsequently, Williams-Boyce and Daniel (1986) found that other mammals could also regenerate ear holes, including chinchillas, cows, pigs, rats, mice, marmosets, stumptail monkeys, and springhares. Ear hole punching is commonly used as a permanent identification method for young laboratory mouse stains due to their inability to close the wound, in this case, they heal by scarring. Using this approach, it was unexpectedly discovered that the MRL mouse strain can close 2-mm-diameter holes by regeneration and not by scarring, establishing an accessible murine model for mammalian regeneration (Clark et al., 1998). Similarly, during a study on aging and immunity, Reines et al., found that ear punches performed in C57BL/6 middle-aged female mice (9-month-old) disappeared after several days. Subsequent studies confirmed that hole punches heal by reconstituting cartilage, muscle, adipose tissue, and pilosebaceous units in both C57BL/6 and Balb/c aged mice strains, although, generally, the hole does not close completely (Reines et al., 2009). Similarly, 2-mm ear holes made in CD1 stock and Balb-c strain middle age female mice healed exhibiting regenerative features such as rapid reepithelialization, formation of a blastema-like structure and re-differentiation of cartilage, muscle, and pilosebaseous units, however, this ear hole closure was not completed, resulting in a partial and resticted re-diferentiation of the involved tissues (Abarca-Buis et al., 2018, 2020). Thus, "limited regeneration" was opted to refer this type of repair where is involved regenerative features but without completing the process (Abarca-Buis et al., 2020). Interestingly, in 18-month-old C57BL/6 female mice, 2-mm ear holes regenerated completely by fusing opposing cartilage end plates (Nishiguchi et al., 2018). These observations contradict the generally accepted view that mammal regeneration declines with age (Sousounis et al., 2014).

Although generally, mammals have lost the ability to promote multiple-tissue regeneration, two species of African spiny mice (*Acomys kempi* and *A. percivali*) have been reported to exhibit skin autotomy, resulting in wounds that heal quickly by a regeneration mechanism. In agreement with this, *Acomys* species were also able to close 4-mm ear punches resulting in new skin formation with pilosebaceous units, adipose cells, and cartilage through blastema-mediated regeneration (Seifert et al., 2012). Therefore, *Acomys* species' capacity for multiple-tissue regeneration and several mammal's abilities to regenerate ear holes have drawn new attention to search for the mechanisms involved in mammalian regeneration. Experiments using mice that lack p21 expression indicated that the p21-C/EBPα transcription factor complex induces the expression of the chemokine *Sdf1* (*Stromal-derived factor 1*) in keratinocytes, which results in the recruitment of CXCR4 positive leukocytes and scar formation in mouse ear holes. Genetic or pharmacological disruption of p21, SDF-1, and CXCR4 decreased fibrosis and promoted regenerative features during ear hole closure (Bedelbaeva et al., 2010; Leung et al., 2015). In addition, age-dependent epigenetic control of *Sdf1* is also involved in regulating fibrosis and scar formation as well as regeneration (Nishiguchi et al., 2018). Moreover, the improvement of healing response by modulation of fibrosis mediated by TGFβ signaling in 2-mm ear punches in 8-month-old female Balb/c mice (Abarca-Buis et al., 2020), highlighting the importance of fibrosis in restricting the regenerative response. Notably, ear hole repair has not been assessed during the early postnatal development of mice, which is characterized by rapid organism growth.

In this work, we evaluated the healing process of the mouse ear along the proximodistal axis. For this, we punched a hole in the middle or proximal regions of pinna and evaluated wound closure and histological features. In addition, we assessed the influence of mouse growth on ear punch repair by performing the wound at postnatal day 21 (PN21), near the end of the early postnatal phase.

2 | METHODS

2.1 | Mice

This study was carried out in accordance with the Guide for Care and Use of Laboratory Animals of the Mexican Official Standard (NOM-062-ZOO-1999), and the protocol was approved by the Mexican Internal Committee for the Care and Use of Laboratory Animals of the Instituto Nacional de Rehabilitación "Luís Guillermo Ibarra Ibarra" (protocol number: 68/20). The number of animals used for each experiment was minimized using well-defined inclusion criteria that were established a priori.

The inbred Balb/cAnNCr strain (RRID:MGI:2160915) was used in this study; this strain has been used previously to study limited regeneration processes in ear holes (Abarca-Buis et al., 2020). The present study used 8-month-old female mice weighing between 25 and 30 g and mice of both sexes on postnatal day (PN) 21 weighing between 10 and 13 g. All mice had anatomically normal ears. The sample size was based on previous works (Abarca-Buis et al., 2020; Costa et al., 2009); we used the minimum sample size to maintain statistical power greater than 80%. Because young mice were obtained from pregnant mice, the number of allocated experimental units was based on the number and sex of all born animals; therefore,

randomization was not used to allocate experimental units. For all experiments, the experimental unit was the individual mouse, and all data points were included in the analysis.

Specific-pathogen-free mice were obtained by Charles River Raleigh through the vivarium of the Instituto de Biotecnología, Universidad Nacional Autónoma de México. All animals were housed under pathogen-free conditions with food and water provided ad libitum; vivarium conditions consisted of 21 ± 2°C, 50% ± 10% relative humidity, and a 12-h light/dark cycle. All animals received the same clinical follow-up, and every hole was performed by the same researcher. A single experimenter was aware of the group's allocation for the different analyses. All procedures were performed in a surgery room of the Instituto Nacional de Rehabilitación "Luís Guillermo Ibarra Ibarra" vivarium. According to the Guide for Care and Use of Laboratory Animals of the Mexican Official Standard (NOM-062-ZOO-1999), the animal handling carried out in this work entails slight stress and short acute pain; the study did not have humane endpoints.

2.2 | Descriptive comparison of non-injured ears

First, we performed a descriptive topographical trial comparing the distal, middle, and proximal regions of the same ear. No control group was used due to the nature of the experiment. Balb/cAnNCr (RRID:MGI:2160915) 8-month-old female mice were anesthetized with inhaled isoflurane and sacrificed by cervical dislocation. Ears were dissected, fixed for 3 days (SAFEFIX II™; Fisher Scientific), and cut into three regions: distal, middle, and proximal (approximately 7.5, 5.5, and 2.5 mm from the external acoustic meatus to the pinna distal tip, respectively). Ear sections were dehydrated and embedded in Paraplast® (Sigma-Aldrich) to obtain 5-μm cross-sections. Sections were stained with Masson's trichrome.

2.3 | Wound healing of 2-mm diameter ear holes

Experimental, descriptive, prospective, and open-label study was performed in all subsequent analyses involving ear damage. Given the descriptive and comparative nature of these experiments, a control group was unnecessary.

First, Balb/cAnNCr (RRID:MGI:2160915) 8-month-old female mice received an ear punch in the distal, middle, and proximal regions; however, ear holes made in the distal portion were excluded a posteriori due to frequent wound tearing. Ear hole closure and proximal ear thickness were compared between middle-aged (8-month-old) and growing (PN21) female mice.

Second, we compared ear wound closure, total ear area, and proximal ear thickness between growing females and males at PN21, 24, 42, and 56. Wounds with irregular edges were excluded from the study because irregular punches affect the regenerative capacity of the ear (Rajnoch et al., 2003). Wounds were performed under inhaled isoflurane anesthesia. A two-millimeter diameter hole was made in the proximal or middle ear regions (proximal, 1 mm; and distal, 4 mm from the external acoustic meatus to the nearest edge of the punch hole) using a thumb punch and a piece of cardboard for support. Wounded ears were dissected after 35 days and fixed. Ears were dehydrated and embedded in paraffin (Paraplast) to obtain cross-sections of 5-μm, which were stained with Masson's trichrome.

2.4 | Morphological evaluation

We used a stereomicroscope (Discovery V20; Carl Zeiss) fitted with a high-speed polychromatic camera (AxioCam; Carl Zeiss) to take pictures of the ears. The complete ear area and wound area were measured using Zen 3.0 blue edition digital image-processing software (Carl Zeiss).

2.5 | Image acquisition and morphometric analysis

Photomicrographs were acquired using an Imager Z1 microscope (Carl Zeiss). For bright-field and fluorescent image acquisition, we used high-speed polychromatic and monochromatic cameras (AxioCam; Carl Zeiss). Ear and cartilage thickness, as well as elongation of the dermal growth, were measured on the acquired images using AxioVision software (ver. 4.8.1.0; Carl Zeiss). Ear volume was calculated by multiplying the area of the complete ear by the thickness of the ear cross-section. Ear area was calculated by Zen 3.0 (blue edition) software (Carl Zeiss) image analysis of pictures obtained with a Discovery stereomicroscope (Carl Zeiss) under 7.5× magnification. Ear cross-section measures were obtained by image analysis of photomicrographs taken with a Z.1 Imager microscope (Carl Zeiss) under 10× magnification using the same software analysis.

2.6 | Immunofluorescence

Blood vessels, neutrophils, macrophages, and Sox-9 were identified by immunofluorescence. Blood vessels were detected using a mouse monoclonal antibody against anti-alpha smooth muscle actin (α-SMA, Cat# ab7817, RRID:AB_262054; Abcam); neutrophils, by an anti-rabbit polyclonal antibody against neutrophil elastase (Abcam; Cat# ab68672, RRID:AB_1658868), Lot#GR286865-3; macrophages, by a rabbit polyclonalCD68 antibody (Abcam; Cat# ab125047, RRID:AB_10971844), Lot#GR192098-3; and Sox-9 by a rabbit polyclonal antibody (Abcam; Cat# ab26414, RRID:AB_778028), Lot#GR91133-1. Cross-sections of the ears (5 μm) were dewaxed and rehydrated. For α-SMA, neutrophil elastase, and Sox-9 detection, the sections were blocked and permeabilized with 1% albumin, 0.3% Triton X100 in phosphate-buffered saline (PBS) for 2 h at room temperature. For CD68 localization, a heat-induced antigen retrieval step using sodium citrate buffer was performed before

blocking with 1% albumin in PBS. Then, slides were incubated at 4°C overnight with the corresponding antibody. After washing, the slides were incubated at room temperature for 2 h with the corresponding secondary antibody as follows: fluorescein F(ab′) 2 fragment of goat anti-mouse IgG (H+L) (Thermo Fisher Scientific; Cat# F-11021, RRID:AB_2536522), Lot#456072 for detection of α-SMA; Goat Anti-Rabbit IgG H&L (Alexa Fluor® 488) antibody (Abcam; Cat# ab150077, RRID:AB_2630356), Lot#GR3375958-2 to localize neutrophil elastase; and DyLight®594 anti-rabbit IgG (Vector Laboratories; Cat# DI-1594, RRID:AB_2336413), Lot#ZE0228 to identify CD68 and Sox-9. Sections were washed three times, mounted with Vectashield® containing 4′,6-diamino-2-phenylindole (DAPI; Vector Laboratories), and cover-slipped. Immunofluorescence-negative controls were obtained by using serum or antibody diluent instead of the primary antibodies. Since skin repair after burning involves immune cell recruitment and blood vessel formation, we used previously burned skin sections as immunofluorescence-positive controls for α-SMA, neutrophil elastase, and CD68. Sections of developing mice digits were used as positive controls to localize chondrogenic progenitors using the anti-Sox-9 antibody.

2.7 | Statistical analyses

Morphometric measures were analyzed using an Unpaired *t*-test or a One-way analysis of variance followed by Tukey's post hoc comparisons for normal distributions. Kruskal–Wallis followed by Dunn's post hoc comparisons were used for non-normal distributions. Statistical analyses were performed using Prism Graph V5.0. Software. Statistical power was determined using SPSS Statistics software. The difference between the compared groups was considered statistically significant when the *p*-value was <0.05.

3 | RESULTS

3.1 | Proximal ear holes show enhanced healing than middle ear holes

To identify differences along the proximodistal axis, histological features were evaluated in the distal (ear tip), middle, and proximal (near to the external auditory canal/acoustic meatus) regions of the ears of adult Balb/c mice. All analyzed regions showed cartilage, dorsal muscle, adipose tissue, pilosebaceous units, and stromal cells embedded in abundant dermal collagen surrounded by a four-cell-layer epidermis (Figure 1a). Pinnae were progressively thicker from the distal to the proximal axis (Figure 1b), partly due to a larger cartilage (Figure 1c,d) and by the presence of more muscle and adipose tissue in the dorsal location (Figure 1c,e). Amplified images of the different tissues constituting the ear showed that the major contributor of the thickening of the proximal region was adipose-associated muscle tissue (Figure 1c). In addition to skeletal muscle, the proximal and middle regions displayed larger blood vessels than distal areas (Figure 2a,b), as revealed by α-SMA$^+$ staining of smooth muscle surrounding arterial walls.

The healing of 2 mm-diameter ear holes in middle-aged females has been regarded as a limited regenerative model in mammals (Abarca-Buis et al., 2020). To identify possible topographical differences in the limited regenerative responses, ear holes were punched in the distal, middle, or proximal regions of the ears of 8-month-old female mice. Unexpected distal injuries were excluded from the study because they frequently tore apart. Thirty-five days post-wound (dpw), the area of the holes made in the middle portion of the ear was significantly larger (Figure 3a,g) than that of the holes made in the proximal region (Figure 3b,g). Proximal wounds exhibited more remarkable regenerative features than middle wounds (Figure 3c–f,h,i), such as more growth of new regenerated structure (Figure 3c,d,h,i) that influenced the cartilage formation. These results indicate that the location of the wound in the proximal-distal axis of the ear influences the limited regeneration process.

3.2 | Mouse growth positively influences the limited regeneration of ear holes

To the best of our knowledge, the ear punch healing response had not been evaluated at the end of the early postnatal phase of mouse development, which is characterized by rapid growth. We analyzed the ears before the injury at PN21 to determine whether they showed completely developed and patterned tissues or still developing tissues. Histological sections of PN21 ears (Figure 4a–c) showed the full arrangement of all tissues present in adult ears, including cutaneous appendages embedded in an organized dermis, muscle, adipose tissue, and cartilage (Figure 4b,c). The appearance of all ear tissues dismissed the possibility that morphogenetic signals influence ear hole healing. Thus, at this stage of postnatal development, the ear is only growing. To evaluate if the growth of the ear influences proximal hole closure, wounds were inflicted in the proximal region of ear pinna of female mice at postnatal day (PN) 21 and 8 months of age. Ear hole area kinetics were compared between these two groups at 1, 3, 5, 7, 14, 21, 28, and 35 dpw. No significant changes in ear hole closure were observed through different timepoints nor between both groups (Figure 4d). However, since ear volume increases twofold from PN21 until the mouse stops growing (Figure 4e), the ear hole area/ear volume ratio was twofold greater at PN21 compared to 8-month-old mice (Figure 4f–h). Ear hole area/ear volume ratio also indicated an accelerated ear hole closure during the first 14 dpw in PN21 ear holes compared to those made at 8-month-old, reaching similar proportions of hole closure until 35 dpw (Figure 4f,i,j). These results suggest that ear growth might contribute to ear hole closure. Histological sections stained with Masson's trichrome at 35 dpw showed the presence of developing elastic cartilage, muscle, and

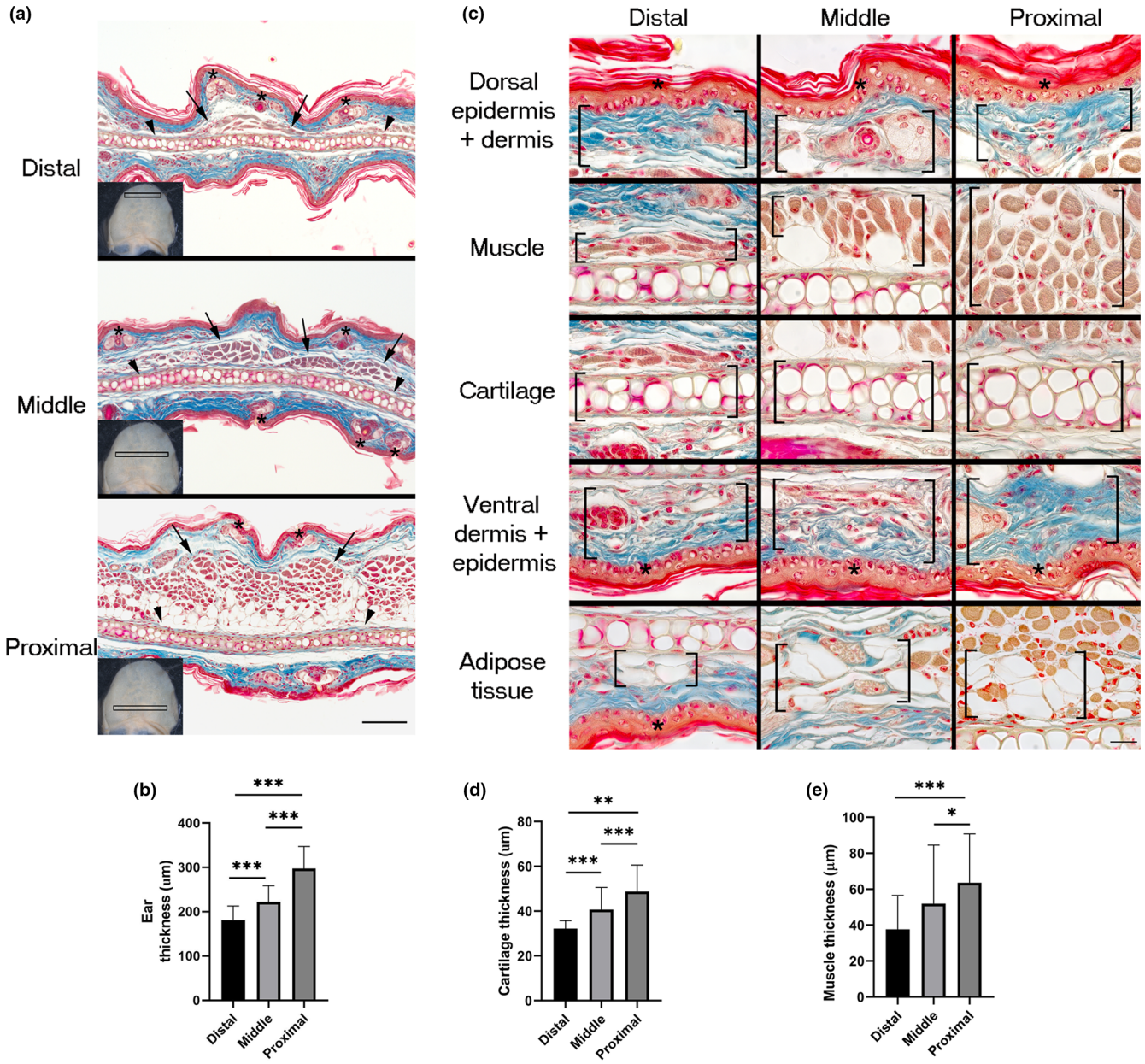

FIGURE 1 Thickness of ear pinna regions. (a) Distal, middle, and proximal regions of the adult mouse ear. Arrowheads, asterisks, and arrows indicate cartilage, pilosebaceous units, and muscle localization, respectively. Analyzed sections were obtained from the regions framed in the ears showed in the left bottom corner of each micrograph. Scale bar = 100 µm. (b) Quantification of ear thickness at distal, middle, and proximal regions. Graphs show mean values ± SD. Ordinary one-way ANOVA was performed ($p < 0.0001$). Tukey's multiple comparison test showed differences among groups indicated with asterisks (***$p < 0.0001$). $n = 5$. (c) Magnified images showing the differences in the thickness of the several tissues that constitute the ear in different regions: Distal, middle, and proximal. Specific tissues are enclosed in square brackets. Asterisks indicate epidermis. Scale bar = 20 µm. (d) Quantification of ear cartilage thickness at distal, middle, and proximal regions. Graphs show mean values ± SD. One-way ANOVA was performed (Kruskal–Wallis test, $p < 0.0001$). Dunn's multiple comparisons test showed differences among groups indicated with asterisks (***$p < 0.0001$, **$p = 0.0082$). $n = 5$. (e) Quantification of muscle thickness at distal, middle, and proximal regions. Graphs show mean values ± SD. One-way ANOVA was performed (Kruskal–Wallis test, $p < 0.0001$). Dunn's multiple comparisons test showed differences among groups indicated with asterisks (***$p = 0.0001$, *$p = 0.0116$). $n = 5$. ANOVA, analysis of variance; SD, standard deviation

pilosebaceous units in the expanded area filling partially the hole (Figure 4k–n). The presence of all well-recognized and organized tissues before the wound and the restricted reconstitution of these tissues by an incomplete ear hole closure after the wound indicates the involvement of a limited regeneration during the ear hole closure at the end of the early postnatal period in mice, similar to the ear injured in the proximal region of 8-month-old mice (Figure 4i). Additionally, the proportional thickness of ears between growing (PN21, 24, 42, and 56) and 8-month-old female mice was calculated (Figure 4o). This ratio was higher at PN21

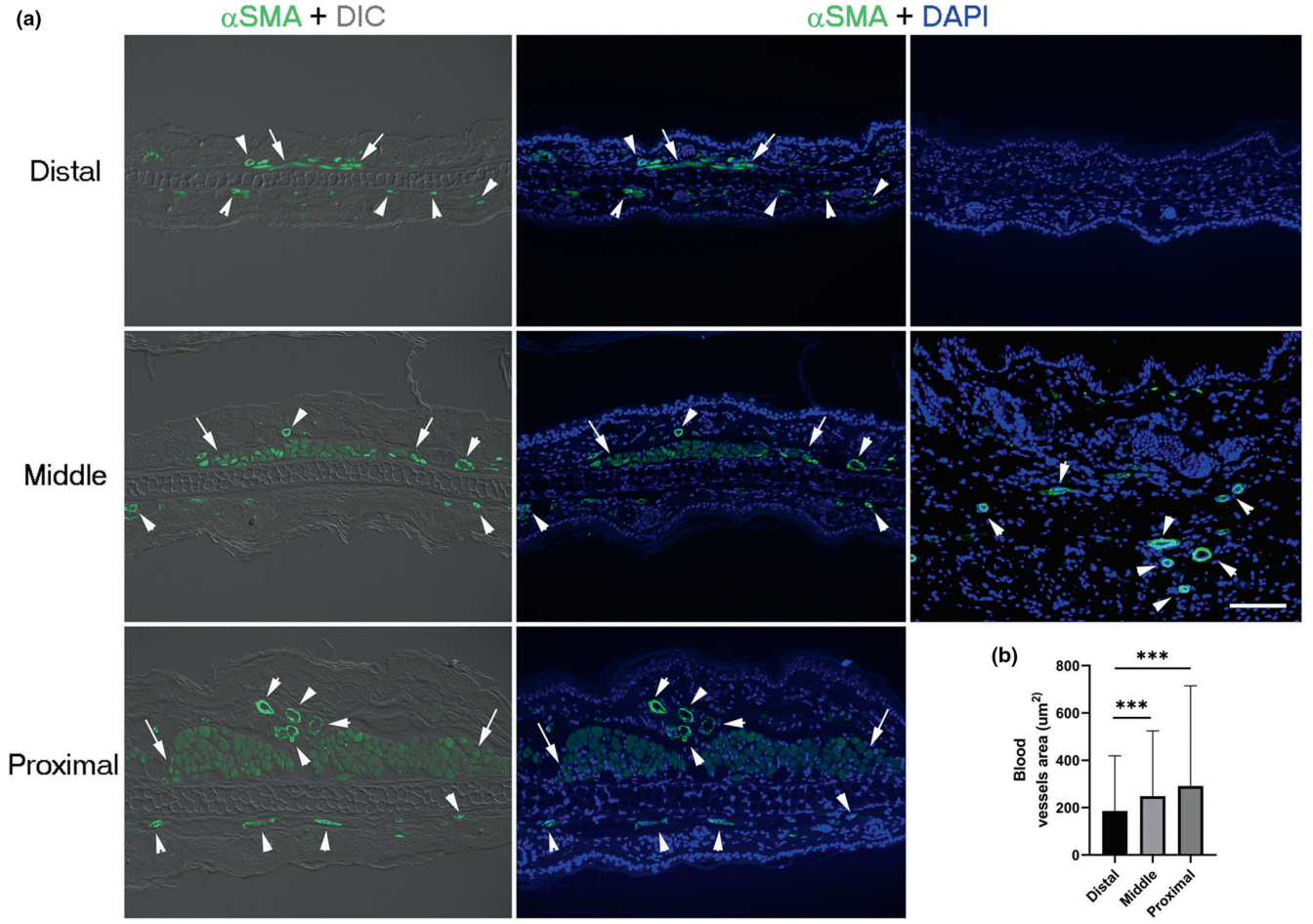

FIGURE 2 Blood vessel size is related to the ear pinna region. (a) Immunofluorescent staining of blood vessels distributed in the distal, middle, and proximal regions of the ear evidenced by staining with α-SMA antibody (green). Left panels show ear sections visualized with differential interference contrast (DIC). The center and right panels show nuclei stained with DAPI (blue). Arrowheads indicate vessels. Scale bar = 100 μm. (b) Blood vessel area in the distal, middle, and proximal ear regions. Graphs show mean values ± SD. One-way ANOVA was performed (Kruskal–Wallis test, $p < 0.0001$). Dunn's multiple comparisons test showed differences among groups indicated with asterisks (***$p < 0.0001$). $n = 5$. Arrows show muscle. α-SMA, alpha-smooth muscle actin; ANOVA, analysis of variance; DAPI, 4′,6-diamino-2-phenylindole; SD, standard deviation

and PN24 and remained constant from PN42 (Figure 4o) to the end of growth, suggesting that ear thickness could improve the limited regenerative response. Ear hole closure kinetics were evaluated in order to find possible differences in the three limited regeneration levels found in this model (high limited regeneration, mild limited regeneration, and scarring). Three inflection points (5, 7, and 14 dpw) were detected when we compared ear hole closure on the proximal region of PN21 and 8-month-old (high limited regeneration) with the middle region of 2- and 8-month-old (scarring and mild limited regeneration, respectively) female mice (Figure 4m). The hole area increased at 5 and 7 dpw in 8- (mild limited regeneration) and 2-month-old (scarring) middle hole respectively (Figure 4p), which suggests the formation of a greater scab that detached these days in comparison to PN21 and 8-month-old proximal hole. The most notable change was observed at 14 dpw, where PN21 and 8-month-old proximal holes showed greater ear hole closure in comparison with the 8-month-old middle hole. In addition, 8-month-old middle hole exhibited a smaller hole than the scarring group (Figure 4p). Overall, our data suggest that high and middle limited regeneration groups have a greater growth of the blastema-like structure that differentiates into the new tissues of the ear. In contrast, the scarring model closed the ear hole more slowly than the other groups and after 14 dpw (Figure 4m).

3.3 | Males and females have similar ear-limited regeneration

To seek sex differences in ear hole closure, we measured the total ear area in females and males at PN21, 24, 42, and 56. No significant differences were found between the groups during the first 8 weeks of age (Figure 5a), indicating a similar growth. The thickness of the proximal ear area was similar between groups, except

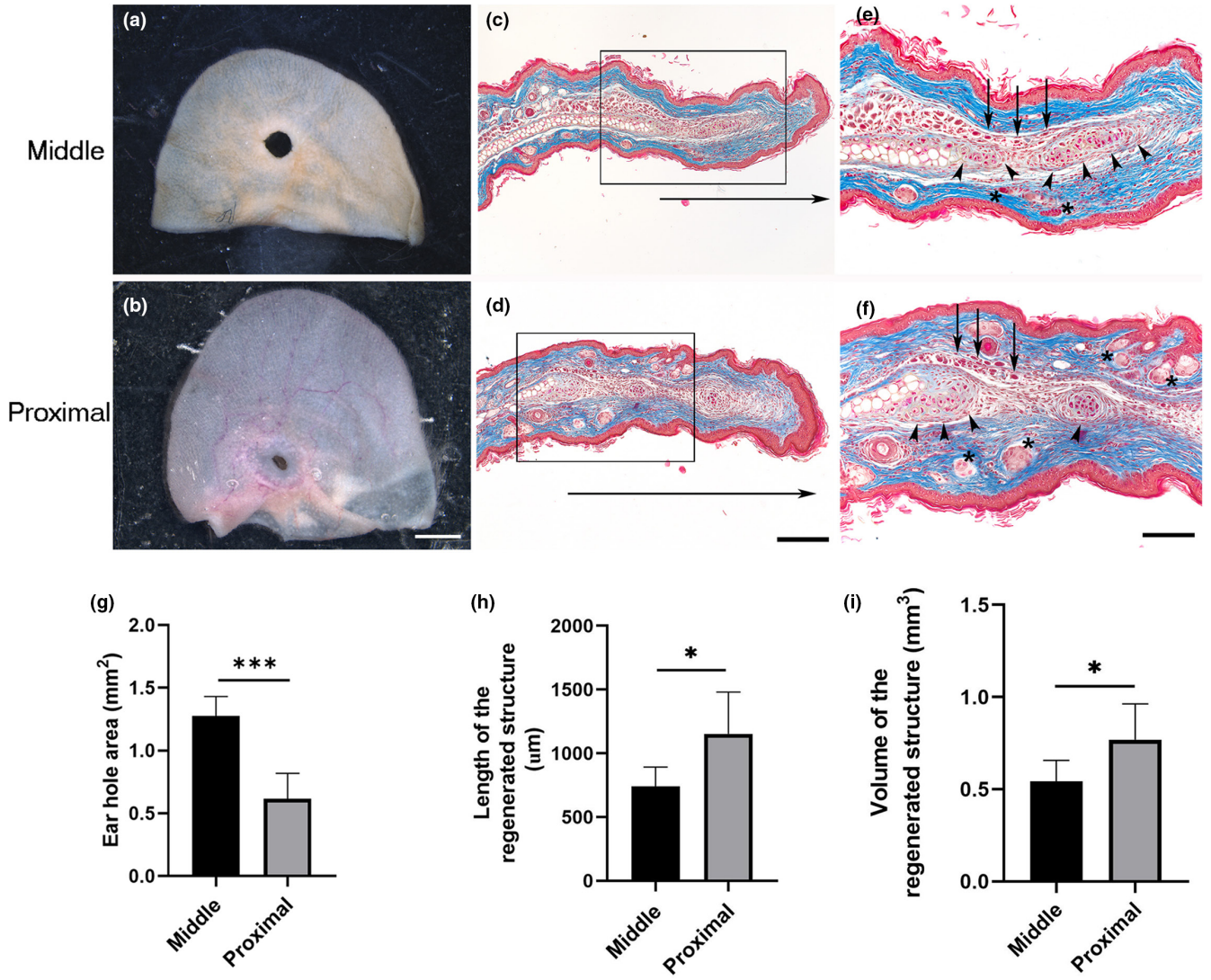

FIGURE 3 Hole punch location influences the limited regenerative response. (a, b) Representative images of ears wounded in the middle or proximal regions from 8-month-old Balb-c female mice at 35 dpw. Scale bar = 2 mm. (c, d) Masson's trichrome staining of healing ear sections punched in the middle and proximal areas at 35 dpw, respectively. Horizontal arrows below sections indicate the growth of newly regenerated structure. Scale bar = 200 μm. (e, f) Magnification of the frame in (c, d), arrowheads, asterisks, and arrows indicate cartilage, pilosebaceous units, and muscle localization, respectively. Scale bar = 100 μm. (g) Ear hole area in the middle ($n = 4$) and proximal ($n = 3$) regions from ears of 8-month-old Balb-c female mice at 35 dpw. Graphs show mean values ± SD. Unpaired *t* test showed differences between both groups (***$p < 0.0001$). (h) Length of the newly regenerated structure at 35 dpw when the hole was made in the middle ($n = 4$) or proximal ($n = 3$) regions of the ear. Graphs show mean values ± SD; unpaired *t* test showed differences between both groups (*$p = 0.0259$). (i) Volume of the regenerated structure at 35 dpw when the hole was made in the middle ($n = 4$) or proximal ($n = 3$) regions of the ear. Graphs show mean values ± SD; unpaired *t* test showed differences between both groups (*$p = 0.0482$). dpw, days post-wound; SD, standard deviation

for PN21 and PN56, where males showed a thicker region compared to females (Figure 5b). This suggests a discontinuous growth in the male ear in relation to the ear thickness. Contrary to previous reports in adult mice (Abarca-Buis et al., 2018; Costa et al., 2009), the younger groups did not display sex differences in hole closure area (Figure 5c–g). Both genders showed de novo formation of cartilage, muscle, and pilosebaceous units in the growing tissue (Figure 5h–k), but males exhibited smaller and less differentiated cartilage nodules in some cases (5/13), suggesting a slight delay in male differentiation.

3.4 | Histomorphological changes during ear hole closure in mice injured during the early postnatal phase

To evaluate the histomorphological changes during ear hole closure, we analyzed histological sections at several dpw. Similar to 8-month-old female mice, PN21 mice had three overlapping limited regenerative stages: wound healing/re-epithelialization, establishment of a blastema-like structure, and re-differentiation.

The first wound-healing/re-epithelialization stage occurred from the moment of injury to 5 dpw (Figure 6a–d). At 1 dpw, there was an infiltration of cells accompanied by an enlargement of the dermis adjacent to the injury. In addition, the re-epithelialization process was noted below the scab (Figure 6a). At 2 dpw, the cell infiltrate persisted, and re-epithelialization was complete in all analyzed samples, forming a thick wound epidermis that lead to the detachment of the scab (Figure 6b). Furthermore, invagination of the wound epidermis contacting the underlying dermis was observed at this time point and persisted at 3 dpw (Figure 6b,c). At 5 dpw, the cell infiltrate was decreased, and the thick wound epidermis presented epidermal ingrowths (Figure 6d).

The second limited regenerative stage started at 7 dpw, with the growth and formation of a blastema-like structure covered by a thick epidermis in the apical region. This blastema-like structure, known as dermal growth, was recognized from the edge of damaged elastic cartilage to the connective tissue underlying the thick wound epidermis and showed multiple undifferentiated cells (Figure 6e).

The re-differentiation stage began at 14 dpw. It was characterized by the formation of cartilage nodules in the blastema-like region, which were generally formed adjacent to the original cartilage. Other processes recognized in this stage include the presence of muscle cells over the nodular cartilage in the dorsal side of ear and some new follicle-sebaceous units in the growing dermal tissue. All these processes occurred in the blastema-like structure and were characterized by low collagen deposition, as observed by the absent blue stain after the Masson's trichrome staining (Figure 6f). Twenty-one days after injury, a larger cartilage lamina was under differentiation, surrounded by a collagenous matrix that occupied most of the newly formed dermis. In addition, we found muscle cells in the proximal region of developing cartilage tissue (Figure 6g). Finally, at 28 and 35 dpw, some regions of the regenerated elastic cartilage displayed hypertrophy, indicating chondrocyte maturation and differentiation. Concomitantly, we observed muscle bundles in the proximal region of the regenerated portion of the ear as well as some pilosebaceous units (Figure 6h,i). To confirm the presence of cells contributing to the formation of new cartilage during the limited regeneration of ear hole, we evaluated the expression of the chondrogenic factor, Sox-9 (Ng et al., 1997). Sox-9 was distributed in the epidermis and pilosebaceous units of the injured ears (Figure 7a). At 7 dpw, some Sox-9$^+$ cells were observed close to the original cartilage at the beginning of blastema-like structure elongation (Figure 7b). At 14 dpw, several Sox-9$^+$ cells were found in the proximal region of the blastema-like structure (Figure 7c). At 21 and 28 dpw, Sox-9 was evident in the regenerating cartilage condensations (Figure 7d,e) until its downregulation at 35 dpw in the hypertrophic cartilage (Figure 7f). Additionally, the same Sox-9 kinetic expression was observed in the wound epidermis at all analyzed times. All these observations demonstrate the high-regenerative ability of the proximal ear region of growing mice.

Due to the importance of neutrophils and macrophages in injury and regeneration (Sindrilaru & Scharffetter-Kochanek, 2013; Wang, 2018), we determined the spatiotemporal distribution of these inflammatory cells. Anti-neutrophil elastase and anti-CD68 antibodies were used to identify neutrophils and macrophages, respectively, during the limited regeneration process of the ear hole of growing mice. Both cell types were found at the early stage of wound healing/re-epithelialization, at 4 hours post-wound (hpw) (Figures 8a and 9a). Neutrophils were located in the clot (Figure 8a,b), where they remained until scab detachment (Figure 8c–f). Macrophages were observed early in both the repairing connective tissue (Figure 9a–c) and fibrin matrix (Figure 9d). CD68$^+$ cells were present in the connective tissue that underlies the wound epidermis picking at 3 dpw (Figure 9e,f). However, macrophages were reduced at the end of the wound healing stage, that is, 5 dpw (Figure 9g). Low macrophage levels were maintained during the establishment of the blastema-like tissue (Figure 9h,i). Finally, some macrophages were observed in the tip of the connective tissue ear during the re-differentiation phase (Figure 9j–l).

4 | DISCUSSION

Although some ear pinnae have complex shapes, their basic anatomic structure resembles a funnel or cone cut in half with dorsoventral (Gawriluk et al., 2016) and proximodistal polarity, where mouse ears exhibit a thicker proximal region. Our histological analysis indicates that thickening is attributed to the abundance of muscle and adipose tissues and to a wider cartilage. In addition, the proximal region showed larger blood vessels compared to medial and distal capillaries.

In this work, we evaluated possible differences between proximal and middle regions regarding ear hole closure. At 35 dpw, there was an improvement in hole closure with traits in the proximal area compared to the middle area. These results agree with studies performed by Williams-Boyce and Daniel (1980, 1986) in several mammalian species, who observed that ear punches placed proximally in the ear could regenerate, as opposed to holes placed in the distal portion. The abundance of muscle and adipose tissue in the proximal region of ear might activate restricted progenitor stem cells in response to the injury. This assumption arises from studies using conditional reporter mouse lines and limb tissue GFP tracking in the axolotl, which demonstrated that the blastema is mostly constituted by fate-restricted progenitor cells derived from the corresponding injured tissues. Thus, the regenerated muscle must come from satellite cells derived from the original muscle tissue (Kragl et al., 2009; Lehoczky et al., 2011).

The thicker cartilage observed in the proximal area of the ear showed a wider perichondrium layer surrounding the elastic

cartilage. The perichondrium is characterized by the presence of cartilage progenitor cells that have even been used for ear cartilage reconstruction (Togo et al., 2006). The presence of a thicker perichondrium in the proximal region of the ear could promote the recruitment of injury-activated cartilage progenitors that contribute to the fully differentiated tissue. In addition, the injury of larger blood vessels in the proximal region in comparsion with distal region could promote the release of blood components, including monocyte-derived macrophages, which are critical for the progression of wound healing (Lucas et al., 2010) and regeneration (Godwin et al., 2013; Simkin et al., 2017). However, ear hole closure at the distal portion could not be assessed in this study because the ear

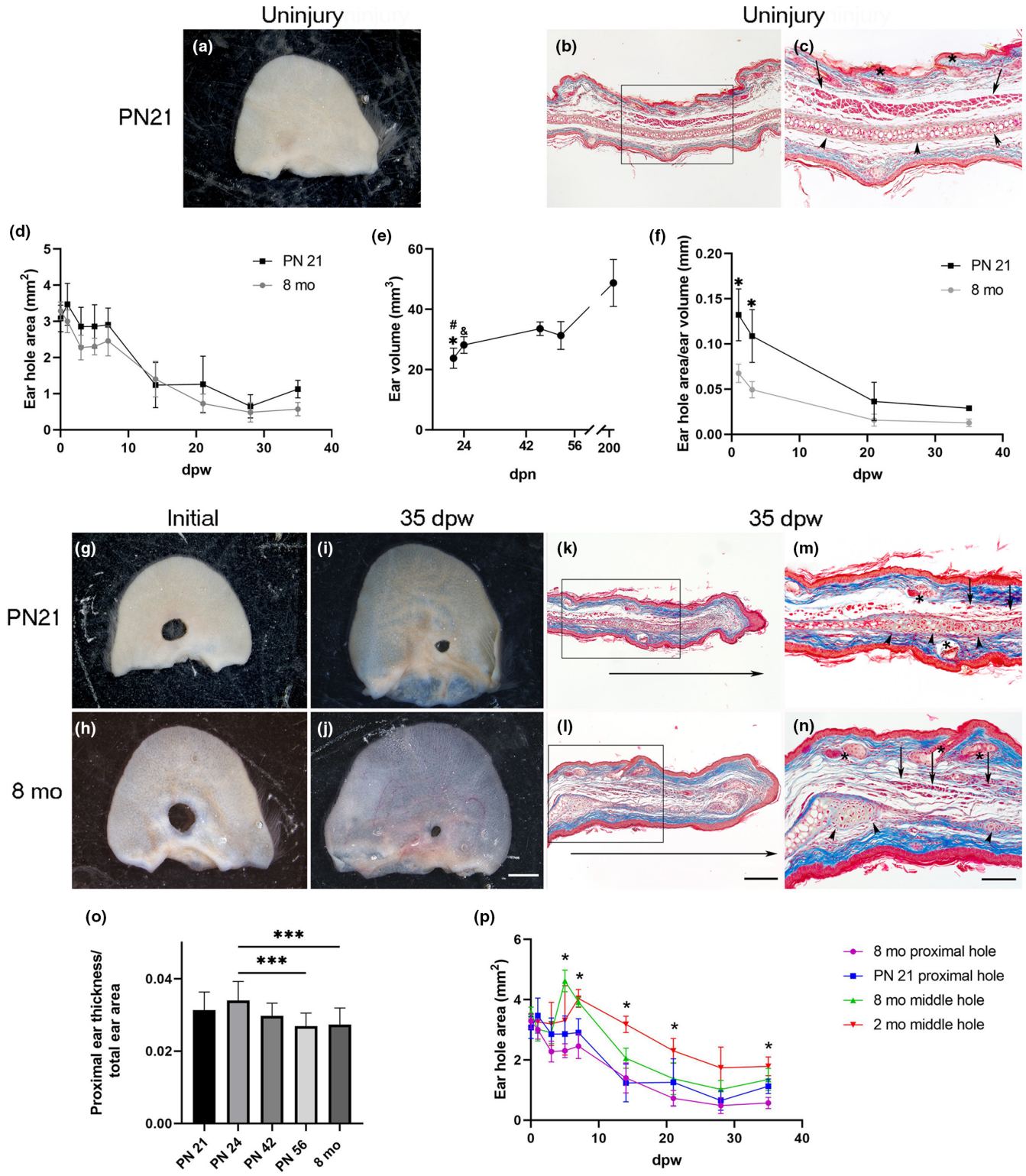

FIGURE 4 Ear closure depends on mice age. (a) Representative image of uninjured ear at PN21. (b) Masson's trichrome stain of uninjured ear section at PN21. (c) Magnification of the frame in (b), arrowheads, asterisks, and arrows indicate cartilage, pilosebaceous units, and muscle localization, respectively. (d) Kinetics of ear hole closure area at 1, 3, 5, 7, 14, 21, 28, and 35 dpw was obtained from female mice injured at PN21 ($n = 3–6$) and 8-month-old ($n = 4–6$). Graphs show mean values ± SD. One-way ANOVA was performed (Kruskal–Wallis test, $p < 0.0001$). However, Dunn's multiple comparison test did not show statistically significant differences among groups at any time. (e) Growth chart in volume of ears obtained at 21, 24, 42, and 56 postnatal day and 8-month-old female mice ($n = 3$). Mice ears showed slight progressive growth during the first 2 months and duplicated their size after 8 months (PN243). Graphs show mean values ± SD. One-way ANOVA was performed (Kruskal–Wallis test, $p < 0.0002$). Dunn's multiple comparison test showed differences among groups: PN21 versus PN42 and 8-month-old ($^{*}p < 0.05$ and $^{\#}p < 0.0001$) and PN24 versus 8-month-old ($^{\&}p < 0.03$). (f) Graphic representation of ear hole area/ear volume ratio at 1, 3, 21, and 35 dpw ($n = 3$). Graphs show mean values ± SD. Statistically significant differences were observed between young and middle age mice during the first 3 days after the wound. p Value for the ordinary one-way ANOVA test was <0.0001, and Tukey's multiple comparison test showed differences between both groups at 1 and 3 dpw ($^{*}p < 0.0005$). (g) Representative images of holes initially made in the proximal region of female mice ear at PN21 (g) and 8-month-old (h). (i, j) Images of hole closure at 35 dpw in female mice that were injured at PN21 (i) and 8-month-old (j). Scale bar = 2 mm. (k, l) Masson's trichrome stain of healing ear sections at 35 dpw of holes made at PN21 (k) and 8-month-old female mice (l). Horizontal arrows below sections indicate the growth of the newly formed tissue. Scale bar in (l) = 200 μm is also applicable to (b, k). (m, n) Magnification of the frame in (k, l), arrowheads, asterisks, and arrows indicate cartilage, pilosebaceous units, and muscle localization, respectively. Scale bar in (n) is also applicable to (c, m). (o) Ratio between the proximal ear thickness and total ear area of growing (PN24, 42, 56) and 8-month-old female mice ($n = 3$). Graphs show mean values ± SD. One-way ANOVA was performed (Kruskal-Wallis test, $p < 0.0001$). Dunn's multiple comparisons test showed differences among groups indicated with asterisks ($^{***}p < 0.0001$). (p) Kinetics of ear hole closure area at 1, 3, 5, 14, 21, 28, and 35 dpw was obtained from female mice injured in the ear proximal region at PN21 ($n = 3–6$) and 8-month-old ($n = 4–6$) and from 2-month-old ($n = 4–6$) to 8-month-old ($n = 3–4$) female mice injured in the middle region. Graphs show mean values ± SD. Mixed-effects analysis was performed followed by Tukey's multiple comparisons test showed differences mainly between the groups at 5, 7, and 14 dpw. ANOVA, analysis of variance; dpw, days post-wound; SD, standard deviation

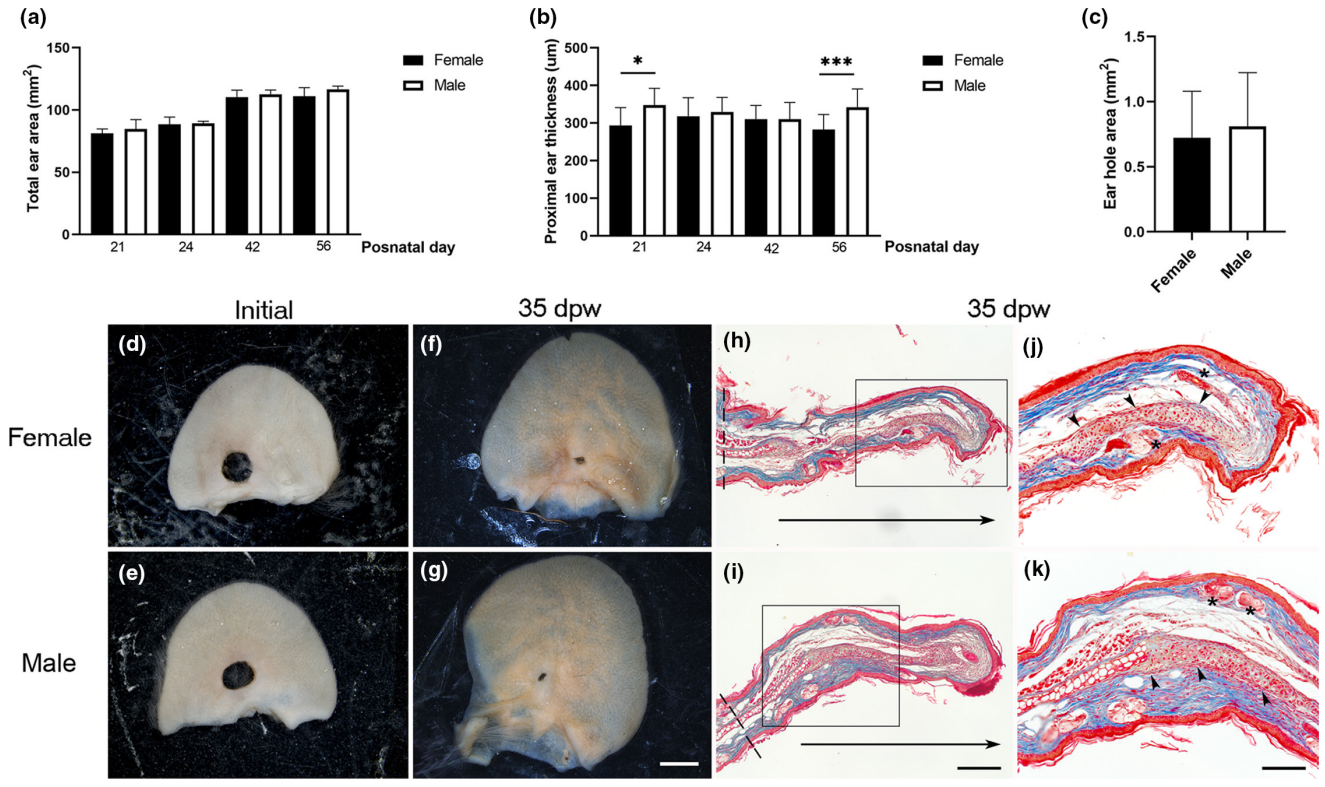

FIGURE 5 The hole closing does not depend on gender. (a) Total ear area of females and males at PN21, 24, 42, and PN56 ($n = 3$). Graphs show mean values ± SD. Ordinary one-way ANOVA showed $p < 0.0001$. Multiple comparisons did not show significant differences between females and males at the same postnatal day. (b) Proximal ear thickness of females and males at PN21 ($n = 3$) graphs show mean values ± SD. Ordinary one-way ANOVA exhibited $p < 0.0001$. Multiple comparisons showed differences among groups indicated with asterisks ($^{*}p = 0.0115$, $^{***}p = 0.0001$). (c) Ear hole area of growing females ($n = 4$) and males ($n = 6$) at 35 days post-wound. Graphs show mean values ± SD. Unpaired t-test was performed. (d, e) Representative images of ears wounded at PN21 in the proximal region of females (d) and males (e). (f, g) Representative images of ear hole closure at 35 dpw in female (f) and male (g) mice. Scale bar = 2 mm. (h, i) Masson's trichrome stain of healing ear sections at 35 dpw of holes made at PN21 in female (h) and male (i) mice. Horizontal arrows below sections indicated the newly formed tissue growth. Dotted lines indicate the ear thickness measured. Scale bar = 200 μm. (j, k) Magnification of the frame in (h, i). Arrowheads and asterisks indicate cartilage and pilosebaceous units, respectively. Scale bar = 100 μm. ANOVA, analysis of variance; dpw, days post-wound; SD, standard deviation

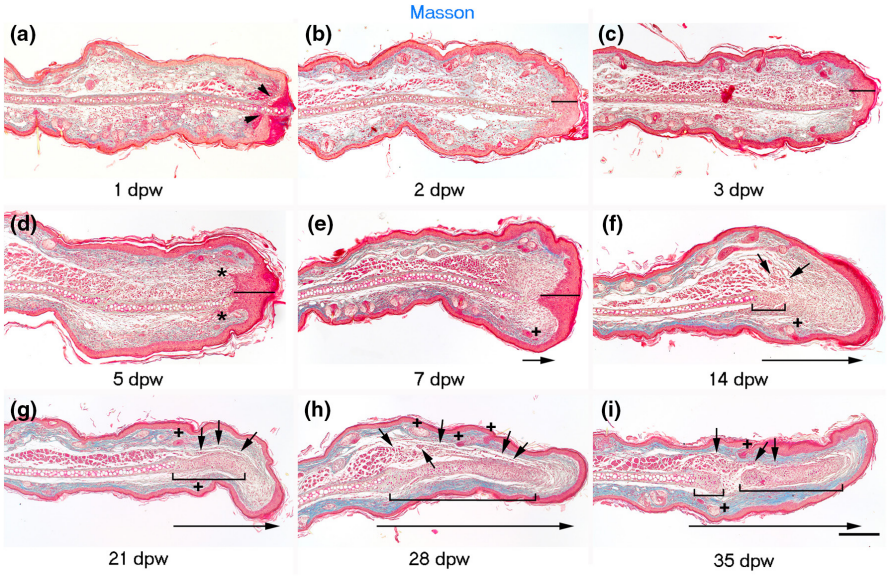

FIGURE 6 Stages of hole closure in mice injured in the proximal region of the ear at PN21. (a–i) Masson's staining at 1, 2, 3, 5, 7, 14, 21, 28, and 35-days post-wound, respectively. Arrowheads in (a) show the wound epidermal margins. Lines in (b–e) indicate the wound epidermis thickness. Asterisks in (d) note epidermal invaginations. + in (e–i) point to forming pilosebaceous units. Short arrows indicate developing muscle in (f–i). Brackets in (f–i) encompass forming cartilage. Long arrowheads indicate the growth of the new tissue. Scale bar = 200 μm.

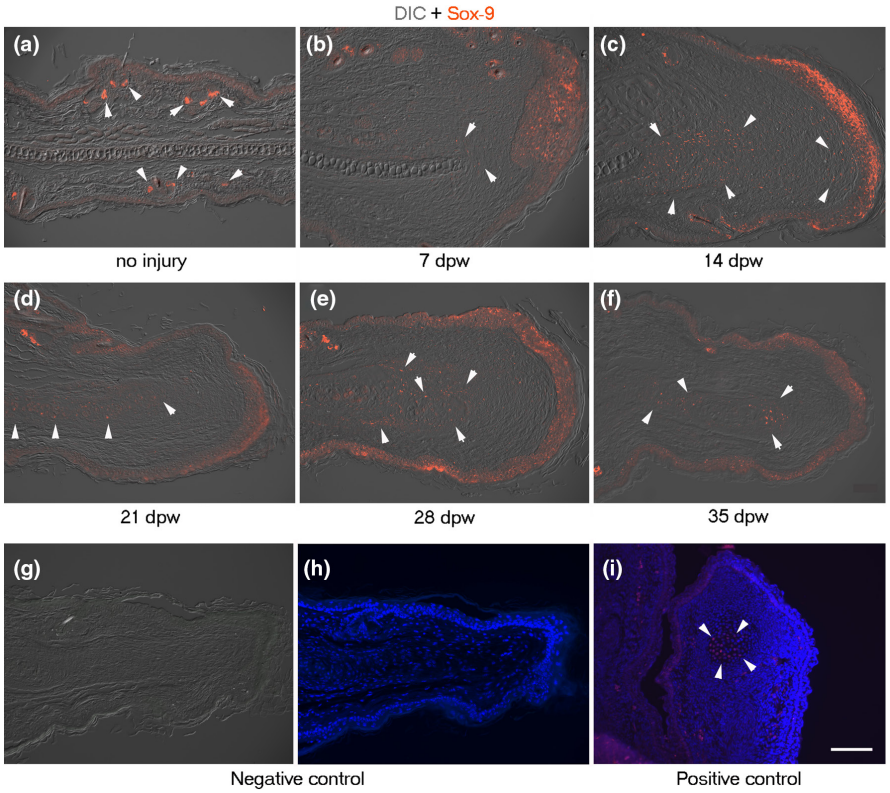

FIGURE 7 Distribution of Sox-9-positive cells during cartilage formation of ear hole closure in female mice wounded at PN21. (a–d, f, g) Sox-9 immunofluorescence (red) ear sections visualized with differential interference contrast (DIC). (a) Presence of Sox-9 in sebaceous glands (arrowheads) and epidermis in non-injured ears at PN21. (b, c) Location of Sox-9 in blastema-like tissue (arrowheads) and wound epidermis at 7 and 14 dpw, respectively. (d–f) Distribution of Sox-9 in cartilage condensations (arrowheads) at 21, 28, and 35 dpw. (g, h) Negative control of Sox-9 immunofluorescence in the regenerating ear at 21 dpw visualized with DIC (g) and DAPI (h). (i) Positive control of Sox-9 immunofluorescence counterstained with DAPI in developing mouse digit tip section at 14 days post coitum. Arrowheads indicate a Sox-9-positive chondrogenic nodule. Scale bar = 100 μm. DAPI, 4′,6-diamino-2-phenylindole; dpw, days post-wound

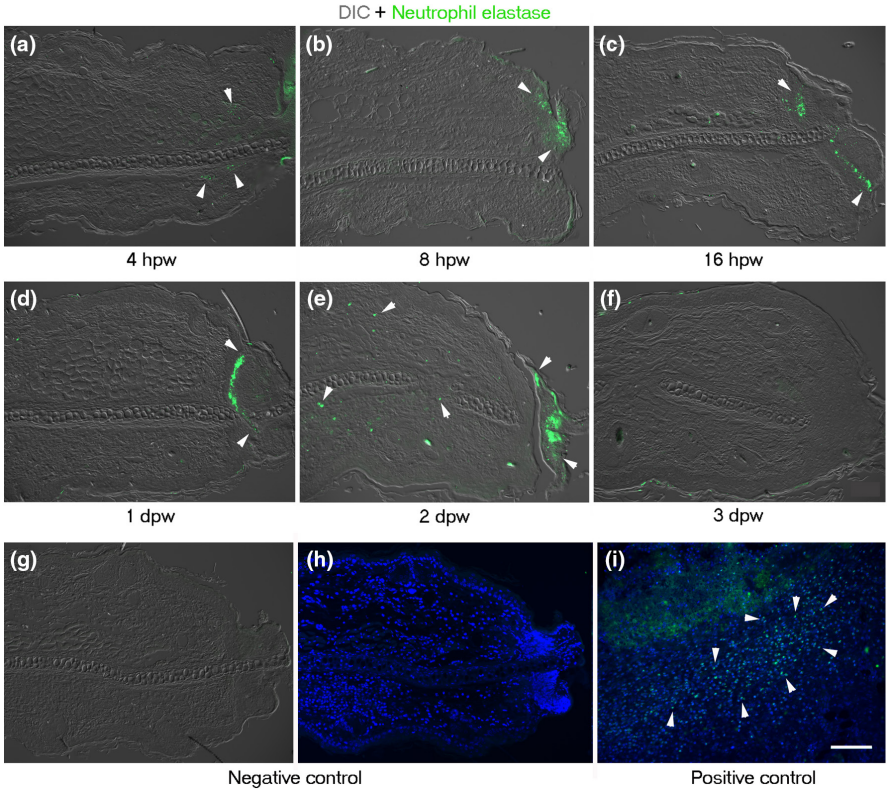

FIGURE 8 Distribution of neutrophils by neutrophil elastase during limited regeneration of ear hole of female mice wounded at PN21. (a–f) Neutrophil elastase immunofluorescence (green) ear sections visualized with differential interference contrast (DIC). (a) Presence of neutrophils in the injury tissue (arrowheads) at 4 hpw. (b) Location of neutrophils in the forming blood clot and necrotic tissue (arrowheads) at 8 hpw. Distribution of neutrophils at the base of the blood clot (arrowheads) at 16 hpw (c), 1 dpw (d), and 2 dpw (e). (f) At 3 dpw, neutrophil elastase$^+$ cells were not detected. (g, h) Negative control of neutrophil elastase immunofluorescence in regenerating ear at 1 dpw visualized with DIC (g) and DAPI (h). (i) Positive control of neutrophil-elastase immunofluorescence in burned mice skin (3 days post-burn) counterstained with DAPI. Arrowheads show neutrophil elastase-positive cells. Scale bar = 100 μm. DAPI, 4′,6-diamino-2-phenylindole; dpw, days post-wound; hpw, hours post-wound

tip tore apart a few days after the punch, possibly due to the slight increase in hole area observed at 5 dpw.

In addition, the contribution of ear growth to ear hole closure was also evaluated. Although the ear hole/ear volume ratio was similar between middle-aged and PN21 mice at the end of the experiment (35 dpw), the ear hole ratio at the moment of the injury was larger in growing mice compared to middle-aged mice, indicating that ear growth contributes to hole closure. Additionally, histological analysis during the ear hole partial closure of early postnatal development mice showed regenerative features indicating that ear growth seems to be essential to promote the limited regenerative response during ear hole repair. Our measurements of total ear volume showed stable ear growth at PN42 and 56, indicating that peak growth is reached during the first month of life. Once maximum growth is reached, the limited regenerative response may be disrupted. In fact, 2-mm ear holes made in 1-month-old mice heal by fibrosis and scar formation (Nishiguchi et al., 2018). These observations suggest that in our model, ear growth occurring after PN21 contributes to the limited regenerative response, but once the ear reaches its definitive size, this process stops. In addition, the histologic analysis revealed that unlike adults, which start the re-differentiation stage at 21 dpw (Abarca-Buis et al., 2020), growing mice begin this stage since 14 dpw. The beginning of this stage is characterized by the presence of Sox-9$^+$ cells in the blastema-like structure and the formation of incipient cartilage nodules close to the edge of the injured cartilage. The histological observations in the subsequent days suggest that the accelerated re-differentiation stage in growing animals results in more developed muscle and a larger and more mature elastic cartilage that expresses Sox-9.

Neutrophils and macrophages are cells of the innate immune system that regulate wound healing and regeneration progress. The location of neutrophils mainly in necrotic area and blood clot suggests a downregulation of their inflammatory activity when this fibrin matrix is detached from the viable tissue by re-epithelialization. Thus, the separation of the inflammatory neutrophil population by this mechanism may lead to the progression of wound healing/reepithelialization phase.

Unlike neutrophils, macrophages were detected during wound healing/reepithelialization and re-differentiation phases. The greater expansion of these cells in the middle wound healing/reepithelialization stage (3 dpw) indicates a higher involvement

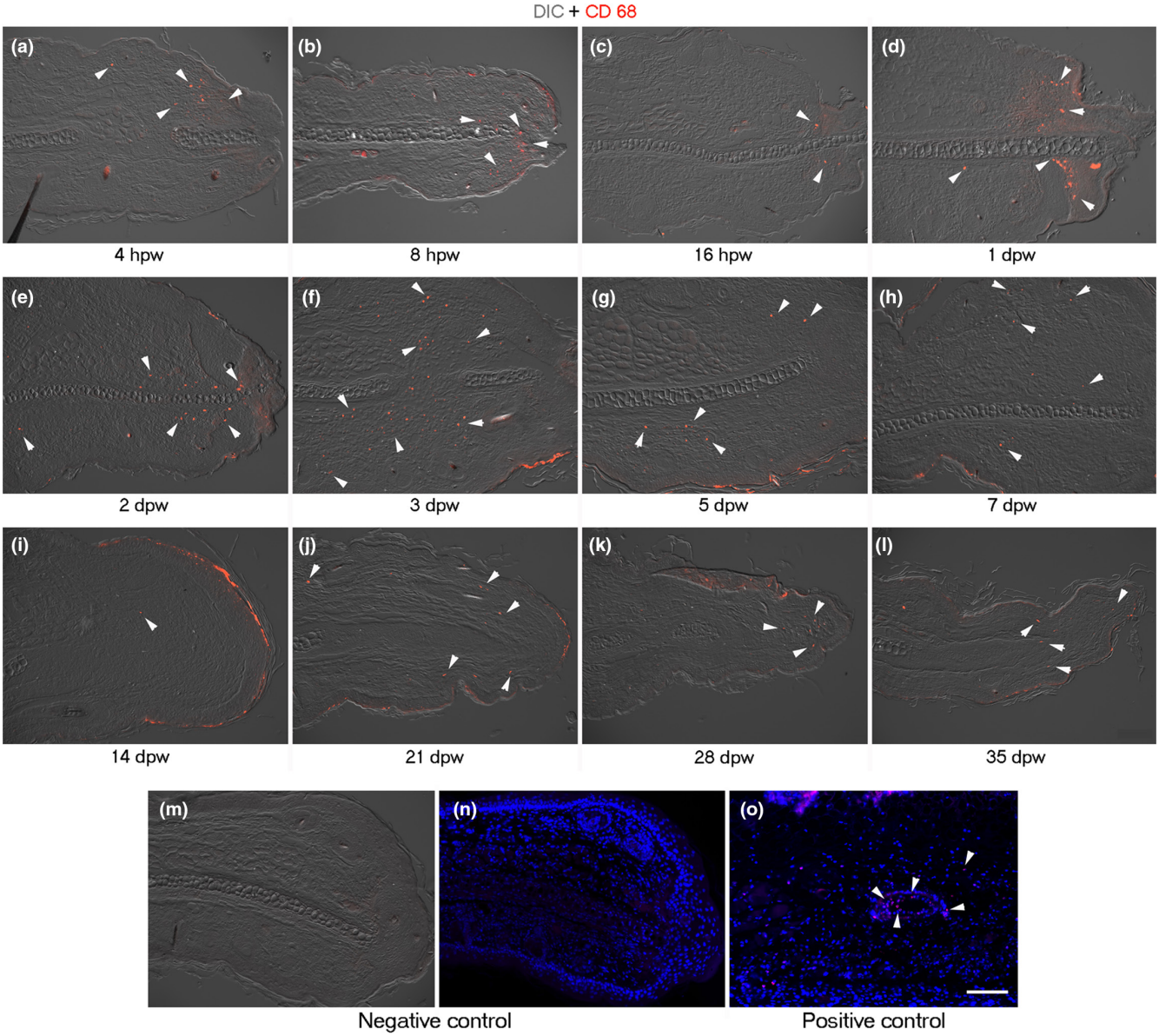

FIGURE 9 Distribution of macrophages by pan macrophages marker CD68 during limited regeneration of ear hole of female mice wounded at PN21. (a–l) CD68 immunofluorescence (red) ear sections visualized with differential interference contrast (DIC). Presence of macrophages in the injury connective tissue (arrowheads) at 4 (a), 8 (b), and 16 hpw (c) and at 1 (d), 2 (e), 3 (f), and 5 dpw (g). A decrease in $CD68^{+}$ cells was noted at the blastema stage at 7 dpw (h) and the beginning of re-differentiation stage at 14 dpw (i) (arrowheads). Macrophages were detected in the middle and late stage of re-differentiation in the tip of regenerating ear at 21 (j), 28 (k), and 35 dpw (l). (m, n) Negative control of CD68 immunofluorescence in the regenerating ear at 3 dpw visualized with DIC (m) and stained with DAPI (n). (o) Positive control of CD68 immunofluorescence in burned mice skin (3 days post-burn) counterstained with DAPI. Arrowheads show CD68-positive cells associated with blood vessel. Scale bar = 100 μm. DAPI, 4′,6-diamino-2-phenylindole; dpw, days post-wound; hpw, hours post-wound

of macrophages in earlier limited regeneration. Macrophages are very plastic cells that change their phenotype according to the environment; at least three different macrophage populations have been recognized during mouse digit tip regeneration (Johnson et al., 2020). The remarkable spatiotemporal distribution of macrophages observed in this work suggests the presence of several subpopulations during the ear hole limited regeneration in growing mice.

It is well known that mammalian regeneration occurs during embryonic development (such as skin and fingertips) and that this ability decreases with age (Ferguson & O'Kane, 2004; Fernando et al., 2011; Han et al., 2003, 2008). In this work, we observed remarkable regenerative traits in growing mice; however, this ability decreases in young animals of 1 and 2 months of age (Nishiguchi et al., 2018; Figure 4g), which is consistent with the concept of age-related regeneration loss. Nevertheless, middle-aged females (8–9 months

old) show regenerative features that reappear in older female mice (18 months old) (Abarca-Buis et al., 2018; Nishiguchi et al., 2018; Reines et al., 2009). Together, these studies indicate a gradual acquisition of regenerative abilities in mice from adulthood to post-reproductive phases. Epigenetic control is key in the regulation of age-dependency regeneration. In 1-month-old mice, ear punches and excisional back wounds induce the secretion of SDF1 by the wounded epidermis, resulting in scar formation. Contrarily, 18-month-old mice, which repair the tissues by regeneration, display low SDF1 levels in both the wounded epidermis and the serum. After injury, aged mice exhibited increased EZH2-mediated H3K27me3 and low H3K4me3 in the promoter and transcription start site of the *Sdf1* gene, resulting in the repression of SDF-1 and regenerative responses (Nishiguchi et al., 2018). Thus, epigenetic changes during postnatal development could influence whether mice repair the wounds through scar formation or regeneration. Together, these observations make the ear hole a valuable model to study all regeneration mechanisms—including position and age-specific ones—in the same system.

Finally, growing male mice showed limited regenerative features unlike young (2 months old) and middle-aged (8 months old) male mice. Commonly, differentiated tissues are not observed during ear hole repair of middle-aged male mice, so they form a scar upon wounding, similar to young males. (Abarca-Buis et al., 2018; Costa et al., 2009). In contrast, we found that growing mice do show a re-differentiation phase, although it was less frequent than in females. It has previously been suggested that male mice heal slowly and poorly compared to females because testosterone prevents complete wound regeneration. This proposal was originated from experiments with castrated Murphy-Roths-Large male mice, which presented hole sizes comparable to those of females (Blankenhorn et al., 2003). These observations suggest that ear hole limited regeneration in males at PN21 could result from sexual immaturity and lack of testosterone production. In addition, the greater proximal thickness of male ears at PN21 could influence the limited regeneration in that region.

In conclusion, two conditions influence the limited regeneration of ear holes in mice: the anatomic position of the punch and ear growth. These observations provide a more comprehensive understanding of this model of mammalian limited regeneration. Translating this knowledge to other non-regenerative mammalian tissues will allow for a more effective response to injuries.

AUTHOR CONTRIBUTIONS

René Fernando Abarca-Buis: Concept/design, acquisition of data, data analysis/interpretation, drafting of the manuscript, approval of the article. **Edgar Krötzsch:** Concept/design, data analysis/interpretation, critical revision of the manuscript, approval of the article.

ACKNOWLEDGMENTS

We thank Ariadna Eusebio García and María Fernanda López González for their excellent technical support, Saúl Renán León Hernandez for his valuable support in statistics and Rebeca Méndez-Hernández for kindly proofreading.

CONFLICT OF INTEREST

The authors have no conflict of interest.

DATA AVAILABILITY STATEMENT

For any underlying research materials as well as data access related to this paper, please contact to René Fernando Abarca Buis. email: buisr@yahoo.com, rabarca@inr.gob.mx.

ORCID

René Fernando Abarca-Buis https://orcid.org/0000-0003-3372-813X
Edgar Krötzsch https://orcid.org/0000-0002-0696-0147

REFERENCES

Abarca-Buis, R., Contreras-Figueroa, M.E., Garciadiego-Cázares, D. & Krötzsch, E. (2020) Control of fibrosis by TGFbeta signalling modulation promotes redifferentiation during limited regeneration of mouse ear. *The International Journal of Developmental Biology*, 64(7-8-9), 423–432.

Abarca-Buis, R.F., Martínez-Jiménez, A., Vera-Gómez, E., Contreras-Figueroa, M.E., Garciadiego-Cázares, D., Paus, R. et al. (2018) Mechanisms of epithelial thickening due to IL-1 signalling blockade and TNF-α administration differ during wound repair and regeneration. *Differentiation*, 99, 10–20.

Bedelbaeva, K., Snyder, A., Gourevitch, D., Clark, L., Zhang, X.M., Leferovich, J. et al. (2010) Lack of p21 expression links cell cycle control and appendage regeneration in mice. *Proceedings of the National Academy of Sciences of the United States of America*, 107(13), 5845–5850.

Blankenhorn, E.P., Troutman, S., Clark, L.D., Zhang, X.M., Chen, P. & Heber-Katz, E. (2003) Sexually dimorphic genes regulate healing and regeneration in MRL mice. *Mammalian Genome*, 14(4), 250–260.

Clark, L.D., Clark, R.K. & Heber-Katz, E. (1998) A new murine model for mammalian wound repair and regeneration. *Clinical Immunology and Immunopathology*, 88, 35–45.

Costa, R.A., Ruiz-de-Souza, V., Azevedo, G.M., Jr., Vaz, N.M. & Carvalho, C.R. (2009) Effects of strain and age on ear wound healing and regeneration in mice. *Brazilian Journal of Medical and Biological Research*, 42(12), 1143–1149.

Ferguson, M.W. & O'Kane, S. (2004) Scar-free healing: from embryonic mechanisms to adult therapeutic intervention. *Philosophical Transactions of the Royal Society of London. Series B, Biological Sciences*, 359(1445), 839–850.

Fernando, W.A., Leininger, E., Simkin, J., Li, N., Malcom, C.A., Sathyamoorthi, S. et al. (2011) Wound healing and blastema formation in regenerating digit tips of adult mice. *Developmental Biology*, 350(2), 301–310.

Gawriluk, T.R., Simkin, J., Thompson, K.L., Biswas, S.K., Clare-Salzler, Z., Kimani, J.M. et al. (2016) Comparative analysis of ear-hole closure identifies epimorphic regeneration as a discrete trait in mammals. *Nature Communications*, 7, 11164.

Godwin, J.W., Pinto, A.R. & Rosenthal, N.A. (2013) Macrophages are required for adult salamander limb regeneration. *Proceedings of the National Academy of Sciences of the United States of America*, 110(23), 9415–9420.

Goss, R.J. & Grimes, L.N. (1972) Tissue interactions in the regeneration of rabbit ear holes. *American Zoologist*, 12(1), 151–157.

Han, M., Yang, X., Farrington, J.E. & Muneoka, K. (2003) Digit regeneration is regulated by Msx1 and BMP4 in fetal mice. *Development*, 130(21), 5123–5132.

Han, M., Yang, X., Lee, J., Allan, C.H. & Muneoka, K. (2008) Development and regeneration of the neonatal digit tip in mice. *Developmental Biology*, 315(1), 125–135.

Heffner, H. & Heffner, R. (2016) The evolution of mammalian sound localization. *Acoustics Today.*, 12(1), 20–27.

Heffner, H.E. & Heffner, R.S. (2018) The evolution of mammalian hearing. *AIP Conference Proceedings*, 1965, 130001. Available from: https://doi.org/10.1063/1.5038516

Johnson, G.L., Masias, E.J. & Lehoczky, J.A. (2020) Cellular heterogeneity and lineage restriction during mouse digit tip regeneration at single-cell resolution. *Developmental Cell*, 52(4), 525–540.e5.

Joseph, J. & Dyson, M. (1966) Tissue replacement in the rabbit's ear. *The British Journal of Surgery*, 53(4), 372–380.

Kragl, M., Knapp, D., Nacu, E., Khattak, S., Maden, M., Epperlein, H.H. et al. (2009) Cells keep a memory of their tissue origin during axolotl limb regeneration. *Nature*, 460(7251), 60–65.

Lehoczky, J.A., Robert, B. & Tabin, C.J. (2011) Mouse digit tip regeneration is mediated by fate-restricted progenitor cells. *Proceedings of the National Academy of Sciences of the United States of America*, 108(51), 20609–20614.

Leung, T.H., Snyder, E.R., Liu, Y., Wang, J. & Kim, S.K. (2015) A cellular, molecular, and pharmacological basis for appendage regeneration in mice. *Genes & Development*, 29(20), 2097–2107.

Lucas, T., Waisman, A., Ranjan, R., Roes, J., Krieg, T., Müller, W. et al. (2010) Differential roles of macrophages in diverse phases of skin repair. *Journal of Immunology*, 184(7), 3964–3977.

Madsen, O. (2009) Mammals (Mammalia). In: Hedges, S.B. & Kumar, S. (Eds.) *The timetree of life*. New York: Oxford University Press, pp. 459–461.

Martin, T., Marugn, T., Ue, J., Vullo, R., Martllo Rel, H., Luo, Z.X. et al. (2015) A cretaceous eutriconodont and integument evolution in early mammals. *Nature*, 526(7573), 380–384.

Martín-Abad, H., Marugán-Lobón, J., Vullo, R., Martin, T., Luo, Z.-X. & Buscalioni, A.D. (2016) *Spinolestes, un mamífero primitivo excepcional del yacimiento de Las Hoyas*. Aragón, España: Fundación Conjunto Paleontológico de Teruel. ISBN: 978-84-944167-3-6, 48 pages.

Ng, L.J., Wheatley, S., Muscat, G.E., Conway-Campbell, J., Bowles, J., Wright, E. et al. (1997) SOX9 binds DNA, activates transcription, and coexpresses with type II collagen during chondrogenesis in the mouse. *Developmental Biology*, 183(1), 108–121.

Nishiguchi, M.A., Spencer, C.A., Leung, D.H. & Leung, T.H. (2018) Aging suppresses skin-derived circulating SDF1 to promote full-thickness tissue regeneration. *Cell Reports*, 24(13), 3383–3392.e5.

Rajnoch, C., Ferguson, S., Metcalfe, A.D., Herrick, S.E., Willis, H.S. & Ferguson, M.W. (2003) Regeneration of the ear after wounding in different mouse strains is dependent on the severity of wound trauma. *Developmental Dynamics*, 226(2), 388–397.

Reines, B., Cheng, L.I. & Matzinger, P. (2009) Unexpected regeneration in middle-aged mice. *Rejuvenation Research*, 12(1), 45–52.

Seifert, A.W., Kiama, S.G., Seifert, M.G., Goheen, J.R., Palmer, T.M. & Maden, M. (2012) Skin shedding and tissue regeneration in African spiny mice (*Acomys*). *Nature*, 489(7417), 561–565.

Simkin, J., Gawriluk, T.R., Gensel, J.C. & Seifert, A.W. (2017) Macrophages are necessary for epimorphic regeneration in African spiny mice. *eLife*, 6, e24623.

Sindrilaru, A. & Scharffetter-Kochanek, K. (2013) Disclosure of the culprits: macrophages-versatile regulators of wound healing. *Advances in Wound Care (New Rochelle)*, 2(7), 357–368.

Sousounis, K., Baddour, J.A. & Tsonis, P.A. (2014) Aging and regeneration in vertebrates. *Current Topics in Developmental Biology*, 108, 217–246.

Togo, T., Utani, A., Naitoh, M., Ohta, M., Tsuji, Y., Morikawa, N. et al. (2006) Identification of cartilage progenitor cells in the adult ear perichondrium: utilization for cartilage reconstruction. *Laboratory Investigation*, 86(5), 445–457.

Wang, J. (2018) Neutrophils in tissue injury and repair. *Cell and Tissue Research*, 371(3), 531–539.

Webster, D.B. (1966) Ear structure and function in modern mammals. *American Zoologist*, 6, 451–466.

Williams-Boyce, P.K. & Daniel, J.C., Jr. (1980) Regeneration of rabbit ear tissue. *The Journal of Experimental Zoology*, 212(2), 243–253.

Williams-Boyce, P.K. & Daniel, J.C., Jr. (1986) Comparison of ear tissue regeneration in mammals. *Journal of Anatomy*, 149, 55–63.

Wolpert, L., Beddington, R., Jessell, T., Lawrence, P., Meyerowitz, E. & Smith, J. (2002) *Principles of development*, 2nd edition. New York: Oxford University Press.

How to cite this article: Abarca-Buis, R.F. & Krötzsch, E. (2023) Proximal ear hole injury heals by limited regeneration during theearly postnatal phase in mice. *Journal of Anatomy*, 242, 402–416. Available from: https://doi.org/10.1111/joa.13782